Atmos. Chem. Phys. Discuss., 13, 26451–26487, 2013
www.atmos-chem-phys-discuss.net/13/26451/2013/
doi:10.5194/acpd-13-26451-2013

Atmospheric Chemistry and Physics Discussions

CLAAS: the CM SAF cloud property dataset using SEVIRI

M. Stengel[1], A. Kniffka[1], J. F. Meirink[2], M. Lockhoff[1], J. Tan[1], and R. Hollmann[1]

[1]Deutscher Wetterdienst (DWD), Offenbach, Germany
[2]Royal Netherlands Meteorological Institute (KNMI), De Bilt, the Netherlands

Received: 5 August 2013 – Accepted: 28 September 2013 – Published: 11 October 2013

Correspondence to: M. Stengel (martin.stengel@dwd.de)

Published by Copernicus Publications on behalf of the European Geosciences Union.

Abstract

An 8 yr record of satellite based cloud properties named CLAAS (CLoud property dAtAset using SEVIRI) is presented, which was derived within the EUMETSAT Satellite Application Facility on Climate Monitoring. The dataset is based on SEVIRI measurements of the Meteosat Second Generation satellites, of which the visible and near-infrared channels were intercalibrated with MODIS. Including latest development components of the two applied state-of-the-art retrieval schemes ensure high accuracy in cloud detection, cloud vertical placement and microphysical cloud properties. These properties were further processed to provide daily to monthly averaged quantities, mean diurnal cycles and monthly histograms. In particular the collected histogram information enhance the insight in spatio-temporal variability of clouds and their properties. Due to the underlying intercalibrated measurement record, the stability of the derived cloud properties is ensured, which is exemplarily demonstrated for three selected cloud variables for the entire SEVIRI disk and a European subregion. All data products and processing levels are introduced and validation results indicated. The sampling uncertainty of the averaged products in CLAAS is minimized due to the high temporal resolution of SEVIRI. This is emphasized by studying the impact of reduced temporal sampling rates taken at typical overpass times of polar-orbiting instruments. In particular cloud optical thickness and cloud water path are very sensitive to the sampling rate, which in our study amounted to systematic deviations of over 10 % if only sampled once a day. The CLAAS dataset facilitates many cloud related applications at small spatial scales of a few kilometres and short temporal scales of a few hours. Beyond this, the spatiotemporal characteristics of clouds on diurnal to seasonal, but also on multi-annual scales, can be studied.

ACPD
13, 26451–26487, 2013

1 Introduction

Cloud property datasets derived from satellite measurements enable global to regional analysis of the spatial and temporal variability of cloud occurrence and specific cloud properties. Different satellite sensor families and types facilitate different analyses and applications due to their individual instrumental characteristics, such as the provided spectral bands or scan modi, or with respect to the time period their measurements are available.

One well established satellite sensor type often used in remote sensing of cloud properties is the passive VIS/IR imager measuring in selected bands in the visible (VIS), near-infrared (NIR) and infrared (IR) part of the electromagnetic spectrum. One example of this type is the Advanced Very High Resolution Radiometer (AVHRR) sensor family, which is flown on NOAA (National Oceanic and Atmospheric Administration) and MetOp (Meteorological Operational Satellite) series of polar-orbiting satellites since more than three decades. Corresponding cloud property datasets are for example the CMSAF cLoud, Albedo and RAdiation dataset version 1 (CLARA-A1; Karlsson et al., 2013) and the AVHRR Pathfinder Atmospheres – Extended version 6 (Patmos-X; Heidinger and Pavolonis, 2009; Heidinger et al., 2010).

In the years 2000 and 2002 the space component of passive VIS/IR imager on polar-orbiting satellites has been enriched by the Moderate Resolution Imaging Spectroradiometer (MODIS) instruments, mounted onboard the polar-orbiting satellites Aqua and Terra, with higher spatial resolution and more spectral bands than precursor instruments (see also Platnick et al. (2003) for MODIS based cloud properties). The most obvious disadvantage of the orbital properties of polar-orbiting instruments is the low temporal sampling rate. A big enhancement in this respect is given by geostationary instruments, which although only measuring parts of the globe, provide observations for all covered regions with high temporal resolution.

Considering the observations of passive VIS/IR sensors in both polar and geostationary orbits, the International Satellite Cloud Climatology Project

ACPD
13, 26451–26487, 2013

(ISCCP, Rossow and Schiffer, 1999) combined correspondingly derived cloud properties in one dataset. This leads to a better spatiotemporal coverage compared to datasets purely based on polar-orbiting sensors. This, however, is at the cost of reduced spectral information due to utilization of the overlapping spectral channels only, which is limited by the older geostationary instruments.

The most advanced, currently existing geostationary passive imager is the Spinning Enhanced Visible and InfraRed Imager (SEVIRI). This instrument has been available since 2003 (its operational phase started in 2004), now available on the third of the Meteosat Second Generation satellites Meteosat-10, in addition to Meteosat-8 and Meteosat-9. Their continuous operational service has created a growing measurement record of nearly one decade. This record now allows for applications with longer temporal scales, going beyond (very-) short-term related applications such as nowcasting.

In this article we present the dataset CLAAS (CLoud property dAtAset using SEVIRI), which contains cloud properties derived from SEVIRI measurements from Meteosat-8 and Meteosat-9 satellites. This work has been done within the framework of the EUMETSAT (European Organisation for the Exploitation of Meteorological Satellites) Satellite Application Facility on Climate Monitoring (CM SAF, Schulz et al., 2009). The intercalibration applied to the visible and near-infrared channels of both SEVIRI instruments creates a solid basis for an homogeneous cloud property dataset. The cloud properties are derived by using two state-of-the-art retrievals schemes. These provide cloud detection, the vertical placement of the cloud and in-cloud properties of optical thickness and effective radius as well as therefrom-derived properties such as thermodynamic phase and cloud water path. The dataset is completed by data summaries for the retrieved cloud variables: the first two moments (on a daily and monthly basis) as well as monthly mean diurnal cycles and histograms. The presented dataset with its high spatial and temporal resolution can serve as mature source for cloud studies in regions covered by the SEVIRI field of view, thus roughly speaking in Europe, Africa, the Atlantic, South America and Middle East. Potential application areas for CLAAS data

ACPD
13, 26451–26487, 2013

also cover regional climate model evaluation or model process studies on, for example, the life cycle and diurnal to seasonal cycles of clouds.

With this article a reference for the CLAAS dataset shall be provided. After an introduction to the topic, the article firstly introduces the SEVIRI instrument and the measurement preparation in Sect. 2. In Sect. 3 we describe the cloud properties considered and summarize the retrieval schemes employed. This is followed by a description of the composition of the dataset in Sect. 4 including the aggregation to higher level products (averages, histograms, mean diurnal cycles). Section 5 summarized the evaluation exercises carried out and in Sect. 6 application examples are given and discussed. Section 7 concludes the article.

2 Satellite data used

2.1 SEVIRI

The SEVIRI instrument (Schmetz et al., 2002) is flown on-board the Meteosat Second Generation satellites Meteosat-8, Meteosat-9 and Meteosat-10, with operational data available from January 2004. It is a passive imager covering the VIS to IR spectrum with its 12 spectral bands, of which three channels are located in VIS, one in the NIR, and 8 in the IR spectrum, with the following nominal centre wave lengths: 0.64, 0.75 (broadband, high resolution visible – HRV), 0.81, 1.64, 3.92, 6.25, 7.35, 8.70, 9.66, 10.80, 12.00 and 13.40 (all in µm). SEVIRI scans the Earth's disk from south to north in approx. 12 min, followed by data processing and transfer, which completes one imaging cycle of 15 min. Not used in this study but carried out for limited time periods and sub regions of the disk are SEVIRI Rapid Scan Services (RSS) with imaging cycles shorter than 15 min. The SEVIRI ground resolution (footprints) near the sub-satellite point (SSP) can in a first approximation be assumed to be of rectangular shape with an edge length of 3 km for all channels, except 1 km for the HRV channel. Due to the scan principle the shape and size of the footprints is not equal over the disk. The east–west

ACPD
13, 26451–26487, 2013

extent of the footprints rapidly increase in zonal direction with distance from SSP; while the same feature is present for the north–south extent of the footprints with increasing meriodonal distance for the SSP (EUMETSAT, 2010). As an example, this results in a footprint size of approximately 4 (east–west extent) by 6 km (north–south extent) over Central Europe. Even though the positions of Meteosat-8, 9 and 10 were similar, they are not exactly identical. After its launch Meteosat-8 was positioned at 3.9° E and after Meteosat-9 became operational at 0.0° in April 2008, Meteosat-8 was moved to 9.5° E. Even though the SEVIRI data projection in Level 1B data is aligned at 0.0° for all satellites, the positions of the individual satellites change SEVIRI's viewing geometries slightly. This is an important feature to consider for each SEVIRI instrument. One needs to keep in mind that observations in same pixels were done under slightly different viewing conditions depended on the time period of observations and the satellite. Also, the field of view (also called SEVIRI disk hereafter) naturally depends on the satellite position. This means that the area covered by the SEVIRI disk is positioned slightly eastwards when SEVIRI on Meteosat-9 took over the operational service.

For the presented dataset the time frame was limited to Meteosat-8 and 9. The covered time period is shown in Fig. 1 together with the operational availability of both instruments and the short term periods for which Meteosat-8 SEVIRI replaced Meteosat-9 due to its maintenance or short term failure. Significant gaps with no data only occurred during the operational service of Meteosat-8 SEVIRI in August 2005 and January 2006, both shorter than 2 days, and September–October 2006, for which a gap of 2 weeks exists. In Fig. 2 the covered area of SEVIRI measurements is shown.

As discussed in Meirink et al. (2013), the operational EUMETSAT calibration of the SEVIRI solar channels deviates from the MODIS instrument on Aqua, which can be considered as one of the best calibrated instruments at present (e.g., Wu et al., 2013). The SEVIRI solar channels were found to be offset by, on average, −8, −6, and +3.5 % for channels 1 (0.6 µm), 2 (0.8 µm), and 3 (1.6 µm), respectively, compared to MODIS-Aqua for the years 2004 to 2009. The temporal trend in these offsets was about 0.5 % per year for channel 1, and smaller for the other channels. The solar channel radi-

ACPD
13, 26451–26487, 2013

ances used for generating the CLAAS dataset were based on the above average inter-calibration results, but the temporal trends were not taken into account, since these had not been properly identified at the time the CLAAS processing started. For the thermal infrared channels the on-board calibration, as provided by EUMETSAT, has been applied.

It is also important to note that recently a new reprocessed SEVIRI radiance dataset became available through EUMETSAT for all SEVIRI data before May 2008. This reprocessed data follows the effective radiance definition, which was already characterizing the radiance data from May 2008 onwards (more details can be found in EUMETSAT, 2008). Using the reprocessed radiance data also for the first part of the CLAAS dataset spanning time period ensures its homogeneity already at radiance level.

3 Considered cloud properties in CLAAS and their retrievals

With respect to the spectral information available through SEVIRI, the following cloud properties were derived for each individual SEVIRI timeslot considered: cloud mask, cloud top pressure (which is also converted into height and temperature), cloud thermodynamic phase, cloud optical thickness and cloud effective radius. The latter two are then used to process liquid and ice water path (LWP, IWP) for each liquid and ice cloud pixel, respectively, also for each individual SEVIRI time slot.

- Cloud mask (CMa), cloud fractional cover (CFC): detecting clouds, meaning identification of those pixels containing clouds, is the basis of nearly all remote sensing applications using visible to infrared spectrum of electromagnetic radiation. For passive imagers, the information content, however, often only allows a binary decision (cloud, clear-sky). For higher level products this information is transferred to cloud fractional coverage by averaging in space and time.

- Cloud-top pressure, height, temperature (CTP, CTH, CTT): these properties are meant to refer to the corresponding properties of the uppermost cloud layer in

ACPD
13, 26451–26487, 2013

a pixel column. The vertical placement of the cloud is, for example, crucial for any cloud type analysis. An exemplary application of cloud top temperature is the radiative effect of clouds in the energy budget.

– Thermodynamic phase (CPh): for passive imagers, detecting the phase at the cloud top is often limited to three classes: liquid, ice, and mixed (of which the mixed class can often not be distinguished). This parameter is needed to determine the cloud type for which optical properties shall be retrieved. Cloud phase retrievals give opportunities e.g. for studying cloud glaciation processes during the development of clouds using temporally highly resolved observations. On climate scales, this allows for analyses on the effects induced by aerosol and dynamics.

– Cloud optical thickness (COT): the vertical integrated optical thickness at 0.6 µm derived in pixels assigned to be cloud filled.

– Effective radius: the particle-surface-area weighted radius of cloud particles. Liquid cloud particles are usually treated as round spheres, while for ice crystals various habits are assumed, given the wide range of shapes occurring in nature such as plates, columns, droxtals and aggregates.

– Cloud water path: this variable refers to the vertical integral of cloud condensate, either for liquid clouds (LWP) or ice clouds (IWP), depending on the retrieved thermodynamic phase at the cloud top.

3.1 MSGv2010

For the detection of clouds and their vertical placement, the MSG NWC software package version v2010 was employed, which was developed within the framework of the EUMETSAT Satellite Application Facility on Support to Nowcasting and Very Short Range Forecasting. The cloud detection is documented in Derrien and Le Gléau (2005) and NWCSAF (2010). In short, the cloud detection is composed of a multi-spectral threshold method during which multiple threshold tests are sequentially ap-

ACPD
13, 26451–26487, 2013

plied. The tests depend on, among others, the illumination (daytime, twilight, nighttime, sunglint) and surface types. Because of these deviating tests, different accuracies can be reached. The output of this procedure is a pixel-based mask with the following levels: non-processed, cloud-free, cloud contaminated, cloud filled, snow/ice contaminated (cloud-free), and undefined. The option of restoring stationary low and mid-level clouds in twilight conditions by carrying forward/backward daylight/nighttime detection information in time (Derrien and Le Gléau, 2010) has been enabled in our processing. The MSGv2010 package also infers the cloud type for each cloudy pixel (Derrien and Le Gléau, 2005; NWCSAF, 2010). This information is, among others, used in the vertical placement of clouds. The vertical placement of the clouds is done via a cloud top pressure retrieval which is dependent on the cloud type. For very low, low, mid-level and high, thick clouds the simulated 10.8 µm brightness temperature is fitted to the measurement by modulating the cloud top pressure including a special treatment of cases with temperature inversions. For high semitransparent clouds, the H_2O/IRW (InfraRed Window) intercept method is applied (Schmetz et al., 1993), which, if not successful, is followed by the radiance rationing method (Menzel et al., 1983). If this method leads to retrieved CTP warmer than the 10.8 µm measurement, the approach as done for thick clouds is used. For fractional clouds no attempt is made to retrieve the cloud top parameters. It needs to be noted that the brightness temperature simulations are done at coarser resolution of 16 by 16 SEVIRI pixels. The radiative transfer model used is the Radiative Transfer Model for TOVS (RTTOV: Eyre, 1991; Saunders et al., 1999). Mandatory atmospheric and surface properties are taken from ERA-Interim reanalysis fields (Dee et al., 2011). The reader is referred to NWCSAF (2010) for more information on the MSGv2010 retrieval package. Figure 2 shows examples of MSGv2010 products, which are discussed in Sect. 4.1.

3.2 CPP

The Cloud Physical Properties (CPP, Roebeling et al., 2006; KNMI, 2012) algorithm uses SEVIRIs VIS and NIR measurements to retrieve cloud optical thickness (COT)

ACPD
13, 26451–26487, 2013

and cloud particle effective radius (REF) by applying the classical Nakajima and King (1990) approach. This approach is based on the basic feature that the reflectance at a non-absorbing wavelength is primarily related to COT, while the reflectance at an absorbing wavelength is mainly related to REF. For SEVIRI retrievals the VIS 0.64 µm and the NIR 1.63 µm channels have been used here as non-absorbing and absorbing channels, respectively. CPP is based on look-up tables (LUTs) of top-of-atmosphere reflectances for plane parallel, single-layer, liquid and ice clouds, simulated by the Doubling Adding KNMI (DAK) radiative transfer model (Stammes, 2001). Spherical water droplets and imperfect hexagonal ice crystals (Hess et al., 1998) have been used in these simulations, respectively. Absorption by atmospheric trace gases is taken into account based on MODTRAN simulations (Berk et al., 2000). For cloudy pixels, as determined by the MSGv2010 cloud mask, COT and REF are retrieved by matching the observed reflectance to the LUTs. First the ice cloud LUT is tried. If this leads to a match and if the cloud top temperature is below 265 K, the thermodynamic phase is set to ice. Otherwise, the water cloud LUT is used, and the phase is set to liquid. Because the retrieval of effective radius for thin clouds is inherently very uncertain, the retrieved effective radius is weighed with a climatological value of 8 micron for water clouds and 26 micron for ice clouds, respectively. The weight of the climatological value is given by a smooth function increasing from 0 at COT $\geq$ 8 to 1 at COT = 0. Liquid or ice water path are then calculated following Stephens (1978):

$$\mathrm{LWP/IWP} = 2/3 \cdot \rho_{\mathrm{l/i}} \cdot \mathrm{REF} \cdot \mathrm{COT}, \quad (1)$$

where $\rho_{\mathrm{l/i}}$ is the density of water and ice, respectively. Equation (1) assumes a vertically homogeneous distribution of cloud condensate. For the retrieved parameters COT, REF, LWP, and IWP, uncertainty estimates are derived by forward propagation of 3 % uncertainty in the VIS and NIR reflectances. Inputs for CPP are the cloud mask from MSGv2010, surface albedo at the VIS and NIR channels based on MODIS data (Moody et al., 2005), and water vapour path from the ERA-Interim dataset. Analysis has shown that cloud property retrievals become very uncertain at high solar zenith

ACPD
13, 26451–26487, 2013

angles (SZA) and viewing zenith angles (VZA). Therefore, no retrievals are performed for SZA or VZA larger than 72°. In addition, because sunglint complicates the retrieval, possibly sunglint-affected pixels over ocean are excluded. CPP has been extensively validated using ground-based observations (e.g., Wolters et al., 2008 and Roebeling et al., 2008). Detailed information on the CPP version used to generate the CLAAS dataset can be found in KNMI (2012).

As for MSGv2010 products, examples of CPP products are shown in Fig. 2 and discussed in Sect. 4.1.

4 Composition of the dataset

The CLAAS dataset is composed of cloud products at different processing levels from pixel-based data to daily and monthly summaries, such as daily and monthly averages and standard deviations as well as monthly mean diurnal cycles and monthly histograms. An overview on the portfolio is given in Table 1. The characteristics of the products of these processing levels are described in the following. It needs to be noted that the spatial coverage of all products of all processing levels undergo an eastward shift after the transition of Meteosat-8 to Meteosat-9 due to the differing satellite positions.

4.1 Pixel-based products

The spatial characteristics of the pixel-based products are identical to the SEVIRI imaging projection and resolution. Thus, the spatial resolution is, as mentioned in Sect. 2.1, approx. 3-by-3 km near the sub-satellite point, with the area generally increasing with satellite zenith angle, the shape however is dependent on the exact position of each pixel (e.g. 4-by-6 km over Central Europe).

Figure 2 shows examples of cloud mask and cloud-top pressure retrievals for the complete SEVIRI disk for one time step. The cloud mask in panel (a) indicates the

ACPD
13, 26451–26487, 2013

clear-sky pixels and pixel containing clouds, whereas the latter is actually separated into two classes: cloudy and cloud-contaminated. In panel (b) the cloud-top pressure is shown, which is derived for pixels characterized as cloudy. In this plot typical cloud regimes can be seen, such as convective systems with low CTP in the Inter-Tropical Convergence Zone (ITCZ) and low strato-cumulus fields off the coast of South-West Africa. In panels (c) to (f) examples of CPP results for cloud thermodynamic phase, cloud optical thickness, and liquid and ice water path are shown. In comparison to the MSGv2010 products, the restriction to a smaller area (zenith angle restriction) is visible. Another limitation is the restriction to cloudy pixels being either liquid or ice. Following this, either liquid or ice water path is retrieved for one specific cloudy pixel.

4.2 Daily and monthly means

For higher level products, a reprojection onto a latitude-longitude grid has been done. This grid spans −90 to 90° in latitude and longitude direction with a grid box size of 0.05° for the averaged products. The (linear) averaging was done on native SEVIRI projection and resolution, which ensures similar observation numbers, followed by a nearest-neighbour reprojection onto the latitude-longitude grid. For CTP an alternative averaging in log-space is done additionally to the linear averaging. The logarithmic averaging approach might be considered for other variables (e.g. COT) as well in future dataset releases. In addition to the all-over daily and monthly means, containing all 24 h slots, cloud fractional coverage is also determined separately for daytime and nighttime conditions. It is important to note that the binary cloud mask values of 0 and 1 are averaged to result in mean cloud fraction. In this averaging procedure, the value of 1 is assigned to the cloud mask class “cloud-contaminated”, which might lead to some overestimation in the averaged products. The pixel-based cloud thermodynamic phase is used to generate daily and monthly mean liquid cloud fraction, which is relative to the number of detected cloudy cases in each grid box in the given time frame. Cloud optical thickness averages are separated into statistics for liquid and ice clouds, which are given additionally to the all-cloud properties.

ACPD
13, 26451–26487, 2013

It is also important to note, that the averages of all cloud properties, except cloud fraction, are in-cloud means. Thus generating all-sky, or grid-mean values, for example for model evaluation, requires the incorporation of the cloud fraction, and possibly also the liquid cloud fraction. For COT, LWP, IWP products in particular the day-time cloud fraction should be used in this respect.

Figure 3 shows monthly averages of cloud fraction, cloud top pressure, liquid cloud fraction, optical thickness, and liquid and ice water path.

4.3 Monthly mean diurnal cycle

Similar to the nominal daily and monthly averaged quantities, a monthly mean diurnal cycle for each cloud property is calculated for each grid cell, which for this products has a width of 0.25° latitude/longitude. Thus, it is of lower spatial resolution than the other cloud products. To compose this products, monthly means are determined for each of the available 24 time steps, separately. For COT the diurnal cycle is determined separately for liquid and ice clouds. It needs to be noted, that even though the diurnal cycle data spans 24 h, cloud products CPh, COT, LWP and IWP are for each grid box only available for daylight conditions.

Figure 4 provides an exemplary case study for CFC and LWP for July 2010. Shown are maps of the amplitude (maximum minus minimum). For this case certain clusters can be found. Highest CFC amplitudes in this month are found for near-coast land regions in South America and Africa in the southern part of the Tropics. Also, the stratocumulus region, exhibits a strong amplitude. Lowest amplitudes are found for ocean regions of the northern and southern mid-latitudes and parts of the Sahara desert. Also shown in Fig. 4 are the representative diurnal cycles for two selected regions (panels c and d). The CFC for the Central European region shows a characteristic feature with a strong diurnal cycle with maximum around 13:00 UTC (14:00 LT) and minimum around midnight. The diurnal cycle for the stratocumulus regions also exhibits a characteristic feature for this region: decreasing cloud fraction during daytime with a minimum in the afternoon. Maximum CFC in this regions lies in the early morning.

ACPD
13, 26451–26487, 2013

The same figure also gives the equivalent visualization for LWP. As seen on the map, the available spatial coverage is reduced. Also, the average diurnal cycle shown for the two selected regions indicate the missing data for non-daylight conditions. Shorter daylight conditions in the selected stratocumulus in this month also further limit the temporal sampling. It is visible that the mean LWP for this regions shows a general decrease during the day between 08:00 and 14:00 UTC. While this is also indicated in the European region after 09:00 UTC, it seems less pronounced. Also, before 08:00 UTC a strong increase is found; while after 14:00 UTC a very strong decrease is found. While the curve for the stratocumulus region reflects a well known feature, the shown European cycle needs to be considered with care. The features seen in the morning and evening in this regions might partly be caused by retrieval artefacts. It needs to be noted that these examples are only snapshots to demonstrate the data. They do not reflect the month to month variability that can be expected due to changing weather regimes, in particular for the European region.

4.4 Monthly histograms

To further provide a better representation of the monthly variability of clouds and their properties, histogram information was composed. Here, all inferred cloud data is collected within a spatial grid box and the number of occurrences is aggregated in specific cloud property bins. For each considered cloud property the binning is defined to span the natural variability but with a limited number of bins which reduces the file size. In case of cloud top pressure the retrieval resolution is also considered. This process resulted in the bin definition for CTP, COT, LWP and IWP as given in Table 2. The bin definitions for CTP and COT include the ISCCP classifications (Rossow and Schiffer, 1999), but with additional subdivisions. COT histograms are additional layered for liquid and ice cloud statistics.

In addition to the one-dimensional histograms, the combinations of CTP and COT were collected and are summarized in two-dimensional histograms (Joint Cloud property Histograms – JCH). Here, the bin definition for CTP and COT is identical to the

ACPD
13, 26451–26487, 2013

one-dimensional histograms, see above. All histograms which include COT, LWP or IWP are limited to daytime data only.

Figure 5 gives an example for the one-dimensional COT histograms for July 2010; aggregated over the full disk and over two selected subregions, Central Europe and a maritime stratocumulus region. Also shown are maps of the relative number of cloud occurrences within two COT ranges (0 to 3.6 and 23 to 100), which were aggregated over the counts of the enclosed bins of the histogram.

Figure 6 gives examples for JCH. Shown are the relative histogram values aggregated over the full disk (panel (a)). Also shown are the spatial distribution of the relative occurrence of (b) cirrus clouds (CTP above 440 hPa and COT between 0 and 3.6 optical thicknesses) and (c) stratocumulus clouds (CTP below 680 hPa and COT between 3.6 and 23 optical thicknesses). The classification for these two clouds types are taken from Rossow and Schiffer (1999). As mentioned above, also this data is collected under daylight conditions only and for satellite zenith angles lower than 72°.

5 Evaluation

The CLAAS products of different processing levels have been validated comprehensively against reference observations from ground based stations (SYNOP, lidar-radar observations) as well as space-borne instruments, such as CloudSat, CALIPSO, AMSR-E. In addition, inter-comparisons have been carried out against the retrieved cloud properties of similar, passive imager instruments (e.g. MODIS). The evaluation results are detailed in Kniffka et al. (2013a) and summarized in the following.

Cloud mask evaluation statistics against CALIPSO and CloudSat reflect the high quality of SEVIRI cloud detection with probabilities of detection around 90 %, while false alarm rates are low with 20 to 28 %. The detection efficiency however significantly depends on the optical thickness of the clouds considered, with detection efficiencies significantly decreasing with decreasing optical thickness below 1.

ACPD
13, 26451–26487, 2013

The accuracy of cloud top retrievals such as the cloud top height and thermodynamic phase was validated using CloudSat and CALIPSO as reference. In short, CLAAS SEVIRI-based CTH retrieval have on average a bias of −1 km considering all clouds. If the sensor sensitivity is considered and the reference CALIPSO height is taken from that cloud level for which the level to cloud layer COT exceeds 0.3, the bias is reduced to −0.6 km. Standard deviations are around 2 km for the filtered subset.

The evaluation of the thermodynamic phase against CALIPSO estimated the probability of detection of ice clouds to be 0.55, while the POD for liquid clouds was significantly higher with 0.82; which indicates a liquid-bias of the phase retrieval. Here however, no COT threshold was applied; and it is assumed that the agreement with CALIPSO would be even better when such a threshold would have been applied to CALIPSO COT profiles, as it was shown for CPP phase retrievals on AVHRR in Stengel et al. (2013). That study also confirms that CPP retrievals of cloud top thermodynamic phase are biased towards liquid phase, in particular for very high, semi-transparent clouds.

COT, LWP and IWP were also compared against MODIS on pixel level. Results show a good agreement between the two products with standard deviation of 6.2 (Bias: 1.8) for optical thickness, 44.9 $g\,m^{-2}$ (Bias: −0.1 $g\,m^{-2}$) for liquid water path and 99.2 $g\,m^{-2}$ (Bias: −6.7 $g\,m^{-2}$) for ice water path.

As mentioned above, the reader is referred to Kniffka et al. (2013a) to infer all details and aspects of the validations done.

It needs to be noted that the accuracy of the derived cloud properties show a dependence on satellite-solar geometries. This is most significant for COT and REF (to a smaller extent) as well as properties derived therefrom. The uncertainties here increase with increasing sun zenith angles.

Another problem, that is caused by the satellite viewing conditions, is the overestimation of cloudiness for large satellite zenith angles due to the slant view. This can lead to increasing systematic errors in higher level products (e.g. monthly means) in this cloud property with increasing zenith angle (increasing distance from the sub satellite point).

ACPD
13, 26451–26487, 2013

Comparisons against SYNOP observations show in this respect an overestimation of 10 % on averages for VZA greater than 70°, which is for example northern Europe. On the other hand, for small VZA the viewing conditions of SEVIRI might actually provide a more accurate measure for the cloud fraction than of the human observer due to its slant observation condition. Averaged over all SYNOP stations within SEVIRI's disk the cloud fraction bias is slightly positive of about 3 %. Moreover, larger satellite zenith angles introduce a representativeness uncertainty for specific pixels, which on average however should not have a significant systematic effect.

Also investigated was the stability of the dataset, which is indicated in Fig. 7. Shown are cloud fraction, liquid cloud fraction and cloud top pressure, all averaged over all pixels within the SEVIRI disk with valid retrievals. This was done for all months and plotted as monthly anomaly from the mean. Also shown are the anomalies for Central Europe. All three parameters exhibit a seasonal cycle, whose amplitudes are similar for each year.

In general the plots suggest that the presented SEVIRI data is fairly stable in time. No significant trend or jump can be seen, despite the transition from Meteosat-8 to Meteosat-9 in 2007 and temporarily back and forth for some Meteosat-9 data gaps afterwards.

6 Exemplary applications of the dataset

In this section we want to highlight the applicability of CLAAS cloud properties, which however will only be of indicative character; more detailed follow-on studies are encouraged for in-depth investigations. One of the strengths of SEVIRI is, as mentioned above, certainly the high frequent measurement sampling for regions covered by its field of view. This enables the observation of spatiotemporally small scale features, which are very present for nearly all clouds and almost all the time, such as the diurnal cylce.

ACPD
13, 26451–26487, 2013

The composition of histograms of cloud properties on short time scale is feasible by the high temporal sampling of SEVIRI. Such histograms, as for example given in Fig. 5, provide an advanced way to reflect the frequency of the occurrences of the cloud properties. Considering the COT histogram in this figure, it becomes obvious that for many regions the COT distribution is dominated by small values up to 3.6 optical thickness; in particular over the Atlantic (except stratocumulus regions) and Indian Ocean, Mediterranean Sea and some spots over South America with values up to 90 %. In this month, clouds with high COT seem to have a significant contribution for European and Central African land, the ITCZ, the mid-latitudes over the Atlantic Ocean, and south-west South America. For the latter regions, this is most pronounced with values up to 20 %. Also very distinct is the difference in histogram skewness between the two selected regions. For Central Europe we find a clear positive skewness with a peak around 3 optical thicknesses. This is in contrast to the stratocumulus region for which the skewness is negative with a peak around 10 optical thicknesses. A more detailed investigation of LWP frequency distribution is documented in Kniffka et al. (2013b).

This investigation indicates that the first two moments are often not enough to sufficiently characterize the cloud variability similarly good for all applications.

Convolving the temporal occurrence of COT with CTP facilitates a cloud type analysis along the lines of the ISCCP (Rossow and Schiffer, 1999). The CLAAS JCH as introduced in Sect. 4.4 accounts for this valuable information on high spatial resolution as well as higher resolution in COT and CTP space. In Fig. 6 the aggregation of this fine-resolved information for two of the classical 9 ISCCP cloud classes is shown: (1) cirrus clouds with COT between 0 and 3.6, and CTP above 440 hPa, and stratocumulus clouds with COT between 3.6 and 23, and CTP below 680 hPa (see also panel (a)). The data is shown as spatial maps of their relative occurrence with respect to the total number of clouds detected in each grid box. In the considered month, cirrus clouds, as defined above, have a high relative occurrence in the tropical Atlantic and Indian Ocean, in addition to some land regions in South America, Middle and northern Africa

ACPD
13, 26451–26487, 2013

as well as eastern Europe and Iberian Peninsula. In contrast to this, stratocumulus clouds have well defined regions of occurrences, i.e. in the subsidence regions of the Atlantic Ocean. In addition, some coastal areas, in particular Africa and eastern South America show similar frequent occurrences of this cloud type. In this context it is very important to notice that with passive imager instruments, such as SEVIRI, usually only the uppermost cloud layer can be identified, thus the occurrences of clouds underneath are not reflected in corresponding cloud property statistics. The joint histograms can also be used to characterize certain weather states and their characteristics, as reported in Rossow et al. (2005) and Oreopoulos and Rossow (2011).

In the following, the strengths of SEVIRI high temporal resolution shall be highlighted. Figure 8 shows the deviations found if cloud properties are only sampled with reduced temporal resolution. For this the monthly mean values based on temporal sampling of 1 (14:00 UTC), 2 (11:00,14:00 UTC) and 4 (9:00,11:00,14:00,16:00 UTC) times per day per grid box were subtracted from the nominal monthly mean; the curves show the histogram of relative deviations for regions between −20° and 20° longitude covered by the SEVIRI disk. For CFC and CTP, also the +12 h values are included, thus the temporal sampling for these are 2, 4, and 8 times per day. The time slots at 11:00 and 14:00 UTC were chosen with respect to the local equator crossing times of MODIS-Terra and AVHRR/NOAA-17 as well as MODIS-Aqua and AVHRR/NOAA-18, respectively. For this example the change in local time over the considered regions is neglected. The other two time slots 09:00 and 16:00 UTC could be seen as another early morning and late afternoon orbits. Table 4 reports standard and mean deviations over the relative differences. A similar investigation, for cloudiness only, is given in Foster and Heidinger (2013).

While a decreasing temporal sampling naturally leads to increasing deviation on average (seen for all cloud variables), for CFC, CTP, and CPh very narrow distributions are found for all subsets. Standard deviations over the relative deviations to the nominal monthly means range for CFC and CTP from 10 to 17 % for 2 daily samples and decrease to 4 to 6 % when using 8 samples. Biases are relative small with values always

ACPD
13, 26451–26487, 2013

below 0.7. In contrast, panels (d) to (f) reveal that the sampling error is much more pronounced for COT, LWP and IWP. Standard deviations for these three variables range from 37 to 55 % when only using 1 sample per day (also indicated by the broad distributions in Fig. 8), which is more pronounced for LWP and IWP than for COT. Partly strong negative biases are found. The values decrease to 18 to 30 % when 4 samples are used. This effect is assumed to be more pronounced for cloud variables which either are very variable in time in general and/or variables which are characterized by a significant diurnal cycle, as it is, for example, indicated in Kniffka et al. (2013b) for LWP.

The benefit of this exercise is twofold. It firstly indicates that SEVIRI based products provide a better estimate of an 24 h mean on daily or monthly basis. Secondly, these numbers can be used to quantify the uncertainties that can be expected for polar-orbiting instruments, such as AVHRR and MODIS if used with this aim.

7 Summary and outlook

In this article we present a cloud property dataset generated within the EUMETSAT Satellite Application Facility on Climate Monitoring and inferred from measurements of the SEVIRI instrument. The dataset spans the time period from 2004 to 2011 using the satellites Meteosat-8 and Meteosat-9, of which the SEVIRI visible and near-infrared measurements were inter-calibrated. Cloud properties considered are cloud mask/fraction, cloud top pressure/height/temperature and the microphysical cloud properties effective radius, optical thickness and thermodynamic phase. The microphysical properties are further utilized to retrieve liquid and ice water path. The properties are inferred on an hourly basis on full SEVIRI spatial resolution, and then further processed on a latitude-longitude grid to compose daily and monthly means as well as monthly mean diurnal cycles and monthly histogram information. Examples of derived cloud properties of different processing levels were shown and discussed. Further, the stability was investigated and shown for cloud fraction, liquid cloud fraction and cloud

ACPD
13, 26451–26487, 2013

top pressure, indicating the stability of the properties over the considered period. In particular the transition between the Meteosat-8 and Meteosat-9 satellites does not cause significant jumps in the time series.

The presented dataset provides accurate cloud property data within the SEVIRI field of view enabling a large variety of applications. Frequency distributions of cloud optical thickness were discussed on an exemplary basis highlighting the capability of SEVIRI to derive mature cloud statistics on small spatial and short temporal scales. Also reported was the uncertainty with respect to reduced temporal sampling, which firstly is minimized when using SEVIRI, and secondly, can be used to quantify corresponding uncertainties for polar-orbiting instruments. While CFC, CTP and CPh show only a small sensitivity, COT, LWP and IWP reveal a strong sensitivity to reduced sampling, which can amount to standard deviations of 55 % when considering relative deviations from the nominal SEVIRI average when considering all pixels in the SEVIRI disk in one month. Also, the mean relative deviation within the disk can exceed 10 %.

Going beyond the indicated areas, numerous further applications will be possible based on this dataset, which are encouraged and envisaged for future studies.

The continuous effort of CM SAF towards composing cloud property datasets based on SEVIRI, as the presented CLAAS dataset, is planned to results in updates in the near future. This will most likely include the extension of the temporal coverage from 01/2004 to 12/2014 with increased temporal resolution of then 15 min. Ongoing collection of user feedback will also impact the selection of cloud properties as well as their technical characteristics in the next dataset edition.

Acknowledgements. This work has been done within the framework of the EUMETSAT Satellite Application Facility on Climate Monitoring (CM SAF). The authors would like to thank the EUMETSAT Satellite Application Facility on Support to Nowcasting and Very Short Range Forecasting for the provision of the MSGv2010 algorithm package. Many thanks also to other CM SAF team members who are not listed as co-authors, but also helped to make this effort succeed.

ACPD
13, 26451–26487, 2013

References

Berk, A., Anderson, G. P., Acharya, P. K., Chetwynd, J. H., Bernstein, L. S., Shettle, E. P., Matthew, M. W., and Adler-Golden, S. M.: MODTRAN4 Version 2 Users Manual, Technical report, Air Force Materiel Command, Air Force Research Laboratory, Space Vehicles Directorate, Hanscom AFB, MA 01731, USA, 2000. 26460

Dee, D. P., Uppala, S. M., Simmons, A. J., Berrisford, P., Poli, P., Kobayashi, S., Andrae, U., Balmaseda, M. A., Balsamo, G., Bauer, P., Bechtold, P., Beljaars, A. C. M., van de Berg, L., Bidlot, J., Bormann, N., Delsol, C., Dragani, R., Fuentes, M., Geer, A. J., Haimberger, L., Healy, S. B., Hersbach, H., Hólm, E. V., Isaksen, L., Kållberg, P., Köhler, M., Matricardi, M., McNally, A. P., Monge-Sanz, B. M., Morcrette, J.-J., Park, B.-K., Peubey, C., de Rosnay, P., Tavolato, C., Thépaut, J.-N., and Vitart, F.: The ERA-Interim reanalysis: configuration and performance of the data assimilation system, Q. J. Roy. Meteor. Soc., 137, 553–597, doi:10.1002/qj.828, 2011. 26459

Derrien, M. and Le Gléau, H.: MSG/SEVIRI cloud mask and type from SAFNWC, Int. J. Remote Sens., 26, 4707–4732, 2005. 26458, 26459

Derrien, M. and Le Gléau, H.: Improvement of cloud detection near sunrise and sunset by temporal-differencing and region-growing techniques with real-time SEVIRI, Int. J. Remote Sens., 31, 1765–1780, 2010. 26459

EUMETSAT: On Differences in Effective and Spectral Radiance MSG Level 1.5 Image Products, EUMETSAT, Am Kavalleriesand, 31, Darmstadt, Germany, EUM/OPS-MSG/TEN/08/0161 v1, 25 April 2008, 2008. 26457

EUMETSAT: MSG Level 1.5 Image Data Format Description, EUMETSAT, Am Kavalleriesand, 31, Darmstadt, Germany, EUM/MSG/ICD/105, 2010. 26456

Eyre, J.: A fast radiative transfer model for satellite sounding systems, ECMWF Tech. Memo. 186, European Centre for Medium Range Weather Forecasts, Shinfield Park, Reading, Berkshire RG2 9AX, UK, 1991. 26459

Foster, M. J. and Heidinger, A.: PATMOS-x: results from a diurnally corrected 30 yr satellite cloud climatology, J. Climate, 26, 414–425, 2013. 26469

Heidinger, A. K. and Pavolonis, M. J.: Gazing at cirrus clouds for 25 years through a split window, Part 1: Methodology, J. Appl. Meteorol. Clim., 48, 1100–1116, 2009. 26453

ACPD
13, 26451–26487, 2013

Heidinger, A. K., Straka III, W. C., Molling, C. C., Sullivan, J. T., and Wu, X.: Deriving an inter-sensor consistent calibration for the AVHRR solar reflectance data record, Int. J. Remote Sens., 31, 6493–6517, 2010. 26453

Hess, M., Koelemeijer, R., and Stammes, P.: Scattering matrices of imperfect hexagonal ice crystals, J. Quant. Spectrosc. Rad., 60, 301–308, 1998. 26460

Karlsson, K.-G., Riihelä, A., Müller, R., Meirink, J. F., Sedlar, J., Stengel, M., Lockhoff, M., Trentmann, J., Kaspar, F., Hollmann, R., and Wolters, E.: CLARA-A1: a cloud, albedo, and radiation dataset from 28 yr of global AVHRR data, Atmos. Chem. Phys., 13, 5351–5367, doi:10.5194/acp-13-5351-2013, 2013. 26453

Kniffka, A., Lockhoff, M., Stengel, M., and Meirink, J. F.: Algorithm Theoretical Basis Document for Cloud Physical Products, EUMETSAT Satellite Application Facility on Climate Monitoring, available at: www.cmsaf.eu, SAF/CM/DWDI/VAL/SEV/CLD, Issue 1, Rev. 1, 2013a. 26465, 26466, 26478

Kniffka, A., Stengel, M., Lockhoff, M., Bennartz, R., and Hollmann, R.: Characteristics of cloud liquid water path from SEVIRI on the Meteosat Second Generation 2 satellite for several cloud types, Atmos. Meas. Tech. Discuss., 6, 8743–8782, doi:10.5194/amtd-6-8743-2013, 2013b. 26468, 26470

KNMI: Algorithm Theoretical Basis Document for Cloud Physical Products, EUMETSAT Satellite Application Facility on Climate Monitoring, available at: www.cmsaf.eu, SAF/CM/KNMI/ATBD/SEVIRI/CPP, Issue 1, Rev. 0, 02 October 2012, 2012. 26459, 26461

Meirink, J. F., Roebeling, R. A., and Stammes, P.: Inter-calibration of polar imager solar channels using SEVIRI, Atmos. Meas. Tech. Discuss., 6, 3215–3247, doi:10.5194/amtd-6-3215-2013, 2013. 26456

Moody, E. G., King, M. D., Platnick, S., Schaaf, C. B., and Gao, F.: Spatially complete global spectral surface albedos: value-added datasets derived from Terra MODIS land products, IEEE T. Geosci. Remote, 43, 144–158, 2005. 26460

Nakajima, T. and King, M. D.: Determination of the optical thickness and effective particle radius of clouds from reflected solar radiation measurements, Part 1: Theory, J. Atmos. Sci., 47, 1878–1893, 1990. 26460

NWCSAF: Algorithm Theoretical Basis Document for "Cloud Products" (CMa-PGE01 v3.0, CT-PGE02 v2.0 & CTTH-PGE03 v2.1), EUMETSAT Satellite Application Facility on Nowcasting and Shortrange Forecasting, SAF/NWC/CDOP/MFL/SCI/ATBD/01, Issue 3, Rev. 0, 17 May 2010, 2010. 26458, 26459

ACPD
13, 26451–26487, 2013

Oreopoulos, L. and Rossow, W. B.: The cloud radiative effects of International Satellite Cloud Climatology Project weather states, J. Geophys. Res.-Atmos., 116, D12202, doi:10.1029/2010JD015472, 2011. 26469

Platnick, S., King, M. D., Ackerman, S. A., Menzel, W. P., Baum, B. A., Riédi, J. C., and Frey, R. A.: The MODIS cloud products: algorithms and examples from Terra, IEEE T. Geosci. Remote, 41, 459–473, 2003. 26453

Roebeling, R., Feijt, A., and Stammes, P.: Cloud property retrievals for climate monitoring: implications of differences between Spinning Enhanced Visible and Infrared Imager (SEVIRI) on METEOSAT-8 and Advanced Very High Resolution Radiometer (AVHRR) on NOAA-17, J. Geophys. Res.-Atmos., 111, D20210, doi:10.1029/2005JD006990, 2006. 26459

Roebeling, R., Deneke, H., and Feijt, A.: Validation of cloud liquid water path retrievals from SEVIRI using one year of CloudNET observations, J. Appl. Meteorol. Clim., 47, 206–222, 2008. 26461

Rossow, W. B. and Schiffer, R. A.: Advances in understanding clouds from ISCCP, B. Am. Meteorol. Soc., 80, 2261–2287, 1999. 26454, 26464, 26465, 26468, 26485

Rossow, W. B., Tselioudis, G., Polak, A., and Jakob, C.: Tropical climate described as a distribution of weather states indicated by distinct mesoscale cloud property mixtures, Geophys. Res. Lett., 32, L21812, doi:10.1029/2005GL024584, 2005. 26469

Saunders, R., Matricardi, M., and Brunel, P.: An improved fast radiative transfer model for assimilation of satellite radiance observations, Q. J. Roy. Meteor. Soc., 125, 1407–1425, 1999. 26459

Schmetz, J., Pili, P., Tjemkes, S., Just, D., Kerkmann, J., Rota, S., and Ratier, A.: An introduction to Meteosat second generation (MSG), B. Am. Meteorol. Soc., 83, 977–992, 2002. 26455

Schulz, J., Albert, P., Behr, H.-D., Caprion, D., Deneke, H., Dewitte, S., Dürr, B., Fuchs, P., Gratzki, A., Hechler, P., Hollmann, R., Johnston, S., Karlsson, K.-G., Manninen, T., Müller, R., Reuter, M., Riihelä, A., Roebeling, R., Selbach, N., Tetzlaff, A., Thomas, W., Werscheck, M., Wolters, E., and Zelenka, A.: Operational climate monitoring from space: the EUMETSAT Satellite Application Facility on Climate Monitoring (CM-SAF), Atmos. Chem. Phys., 9, 1687–1709, doi:10.5194/acp-9-1687-2009, 2009. 26454

Stammes, P.: Spectral radiance modelling in the UV-visible range, in: IRS 2000: Current Problems in Atmospheric Radiation, edited by: Smith, W. L. and Timofeyev, Y. M., 385–388, A. Deepak, Hampton, Va, 2001. 26460

ACPD
13, 26451–26487, 2013

Stengel, M., S., M., Jerg, M., Karlsson, K.-G., Scheirer, R., Maddux, B., Meirink, J., Poulsen, C., Siddans, R., Walther, A., and Hollmann, R.: The Clouds Climate Change Initiative: the assessment of state of the art cloud property retrieval schemes applied to AVHRR heritage measurements, Remote Sens. Environ., accepted, 2013. 26466

Stephens, G.: Radiation profiles in extended water clouds, II: Parameterization schemes, J. Atmos. Sci., 35, 2123–2132, 1978. 26460

Wu, A., Xiong, X., Doelling, D. R., Morstad, D., Angal, A., and Bhatt, R.: Characterization of Terra and Aqua MODIS VIS, NIR, and SWIR spectral bands' calibration stability, IEEE T. Geosci. Remote, 51, 4330–4338, doi:10.1109/TGRS.2012.2226588, 2013. 26456

ACPD
13, 26451–26487, 2013

Table 1. Overview of CLAAS cloud products (indicated by "y") per cloud variable and processing level: pixel-based products (Pixel b.), daily mean (DM), monthly mean (MM), monthly mean diurnal cycle (MMDC), and monthly histograms (MH stands for one-dimensional histograms, JCH for two-dim. COT/CTP histograms). Subscript $_{dn}$ indicates if an additional separation for day and night time values is available and $_{li}$ stands for an additional separation for liquid and ice clouds.

	Pixel b.	DM and MM	MMDC	MH	2dim-H
CFC	–	y_{dn}	y	y	–
CTP, CTH, CTT	y	y	y	y	–
CPh	y	y	y	–	–
COT	y_{li}	y_{li}	y_{li}	y_{li}	–
LWP	y	y	y	y	–
IWP	y	y	y	y	–
JCH	–	–	–	–	y_{li}
Spat. resolution	3–5 km	0.05°	0.25°	0.05°	0.25°
Projection	SEVIRI	lat/lon	lat/lon	lat/lon	lat/lon

ACPD
13, 26451–26487, 2013

Table 2. Bin borders of CLAAS histograms of cloud top pressure (CTP), cloud optical thickness (COT), liquid water path (LWP), ice water path (IWP), and Joint Cloud property Histogram (JCH).

CTP [hPa]	1, 90, 180, 245, 310, 375, 440, 500, 560, 620, 680, 740, 800, 875, 950, 1100
COT	0, 0.3, 0.6, 1.3, 2.2, 3.6, 5.8, 9.4, 15, 23, 41, 60, 80, 100
LWP [$g\,m^{-2}$]	0, 5, 10, 20, 35, 50, 75, 100, 150, 200, 300, 500, 1000, 2000, > 2000
IWP [$g\,m^{-2}$]	0, 5, 10, 20, 35, 50, 75, 100, 150, 200, 300, 500, 1000, 2000, > 2000
JCH	See COT and CTP bins

ACPD
13, 26451–26487, 2013

Table 3. Summary of evaluation scores for CLAAS products as there are given in Kniffka et al. (2013a). Processing level L2 stands for pixels-based products, while L3 refers to monthly averages. The values of standard deviations and biases are reported. Subscripts Hc and Fc refer to hitrate an false alarm for cloud detection. Similarily, Pl, Pi are the probabilities of detection for liquid and ice clouds, while Fl, Fi are corresponding false alarm rates. L2 comparison results for COT, LWP and IWP against MODIS were, in contrast to Kniffka et al. (2013a), extended to cover one month of collocations.

Cloud variable	Processing level	Evaluation source	Evaluation scores (Std/Bias)
CMa	L2	CALIPSO	$0.9^{Hc}/0.2^{Fc}$
CFC	L3	SYNOP	14 %/3 %
	L3	MODIS	9 %/2 %
CTH	L2	CALIPSO	2.0 km/−0.7 km
CPh	L2	CALIPSO	$0.82^{Pl}/0.38^{Fl}$
	L2	CALIPSO	$0.55^{Pi}/0.23^{Fi}$
	L3	MODIS	0.11/−0.03
COT	L2	MODIS	6.2/1.8
	L3	MODIS	32.4 %/−9.9 %
LWP	L2	MODIS	$44.9\,g\,m^{-2}/-0.1\,g\,m^{-2}$
	L3	MODIS	33.6 %/−0.3 %
IWP	L2	MODIS	$99.2\,g\,m^{-2}/-6.7\,g\,m^{-2}$
	L3	MODIS	37.8 %/−6.2 %

ACPD
13, 26451–26487, 2013

Table 4. Sampling uncertainty given in relative standard (std) and mean (bias) deviation over SEVIRI's disk. All values are given in % and were calculated for 1 (14:00 UTC), 2 (11:00,14:00 UTC) and 4 (9:00,11:00,14:00,16:00 UTC) samples per day. For CFC and CTP also the +12 h slot was included, thus the sampling for these two variables contain 2, 4 and 8 samples.

Cloud variable	Uncertainty with 1(2) sample (Std/Bias)	Uncertainty with 2(4) samples (Std/Bias)	Uncertainty with 4(8) samples (Std/Bias)
CFC	16.8/0.6	11.1/−0.7	6.2/−0.4
CTP	10.3/0.4	7.8/0.2	4.7/−0.1
CPh	19.3/1.4	14.4/1.7	10.6/0.2
COT	37.9/−9.9	27.5/−5.3	18.3/1.5
LWP	48.6/−11.8	35.9/−5.1	24.1/1.7
IWP	55.3/1.6	40.6/0.2	30.1/2.1

ACPD
13, 26451–26487, 2013

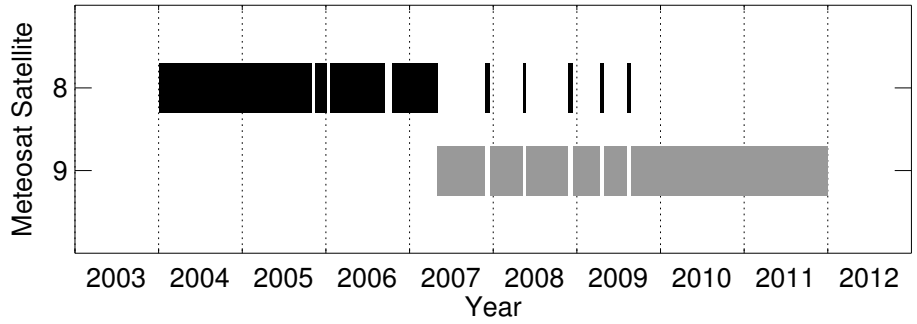

Fig. 1. Temporal coverage of Meteosat-8/SEVIRI and Meteosat-9/SEVIRI measurements as taken in operational service and as used as basis for the presented CLAAS dataset. Gaps in Meteosat-9/SEVIRI measurements are filled with Meteosat-8/SEVIRI data if exceeding one day. Gaps in the Meteosat-8/SEVIRI record remain unfilled.

ACPD
13, 26451–26487, 2013

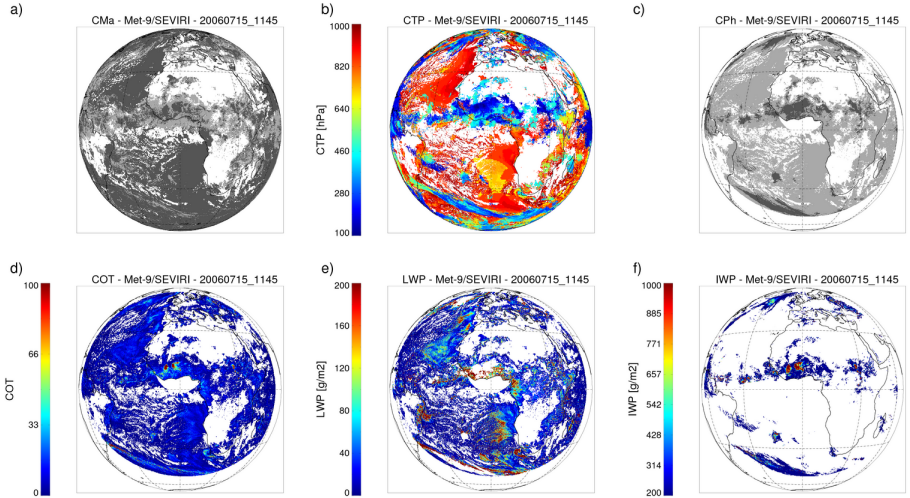

Fig. 2. Examples of pixel-based CLAAS products for **(a)** cloud mask (CMa), **(b)** cloud-top pressure (CTP), **(c)** cloud thermodynamic phase (CPh), **(d)** cloud optical thickness (COT), **(e)** liquid water path (LWP), and **(f)** ice water path (IWP). For the cloud mask plot, dark grey is cloud filled and light gray cloud contaminated. For cloud phase, light grey stands for liquid clouds and dark grey for ice clouds. While for CMa and CTP products are processed at the full SEVIRI field of view, the retrieved optical properties REF and COT (and therefrom derived products CPh, LWP, IWP) are restricted to satellite zenith angles smaller than 72°. Water surface regions contaminated with sun-glint are also omitted. All products are on native SEVIRI projection and resolution and shown for 15 July 2006 at 11:45 UTC.

ACPD
13, 26451–26487, 2013

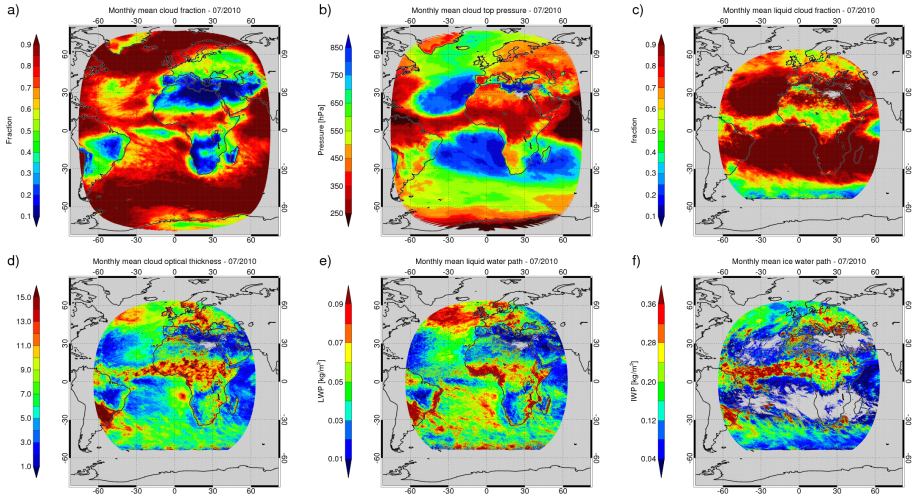

Fig. 3. Examples of monthly averaged CLAAS products for **(a)** cloud fraction (CFC), **(b)** cloud-top pressure (CTP), **(c)** liquid cloud fraction (CPh), **(d)** cloud optical thickness (COT), **(e)** liquid water path (LWP) and **(f)** ice water path (IWP). As for the pixel-based products the optical properties REF and COT (and therefrom derived products CPh, LWP and IWP) are restricted to satellite zenith angles smaller than 72°. All averaged products stand for in-cloud averages. Together with the histograms the averaged products are defined on a latitude-longitude grid with a grid box size of 0.05°. All data is for July 2010.

ACPD
13, 26451–26487, 2013

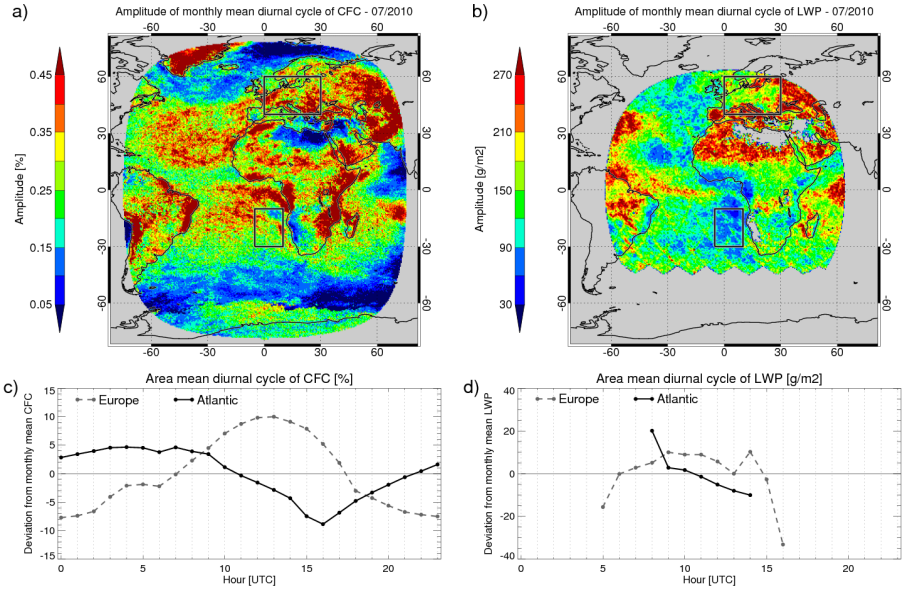

Fig. 4. Exemplary maps of monthly mean diurnal cycle of cloud fraction (CFC, panel **(a)**) and liquid water path (LWP, panel **(b)**, this data was smoothed over 3 neighbouring pixels to better visualize large scale features). Shown are the respective amplitude (maximum minus minimum) for each grid box. In the bottom panels, the average values as function of the time of day for selected regions are shown. The locations of the regions are indicated in the maps. LWP mean values for selected regions exist only during daylight conditions and are only shown for hours for which the entire regions were under daylight conditions. All data is for July 2010.

ACPD
13, 26451–26487, 2013

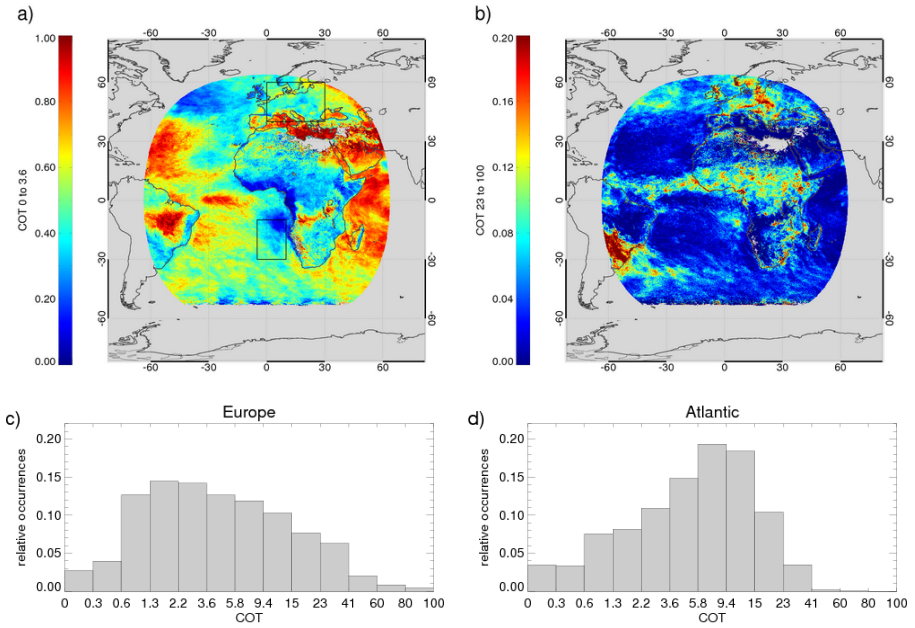

Fig. 5. Top panels show maps of relative occurrence of clouds with cloud optical thickness (COT) between 0 and 3.6 **(a)** and between 23 and 100 **(b)**. The values were normalized with the total number of clouds in each grid box. Panel **(c)** reports the histogram of COT aggregated over a Central European region and panels **(d)** the equivalent for the maritime stratocumulus off the coast of Angola. The regions are indicated in panel **(a)**. All data is for July 2010.

ACPD
13, 26451–26487, 2013

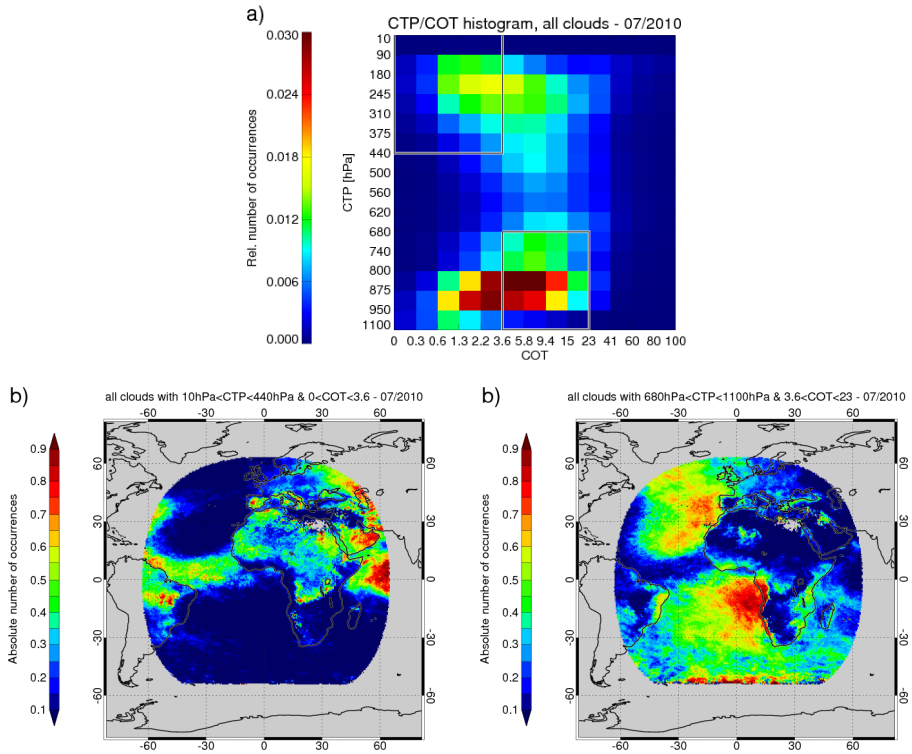

Fig. 6. (a): Joint Cloud property Histogram (JCH) when aggregated over the covered disk (as shown in panels **(b)** and **(c)**). The values have been normalized with the total number of cloud occurrences. **(b)**: Relative number of occurrences of cirrus clouds (as defined in Rossow and Schiffer, 1999) with CTP between above 440 hPa, and COT between 0 and 3.6. **(c)**: Relative number of occurrences of stratocumulus clouds with CTP below 680 hPa, and COT between 3.6 and 23. All data is for July 2010. Grey shaded areas mark regions without cloud observation in this month.

ACPD
13, 26451–26487, 2013

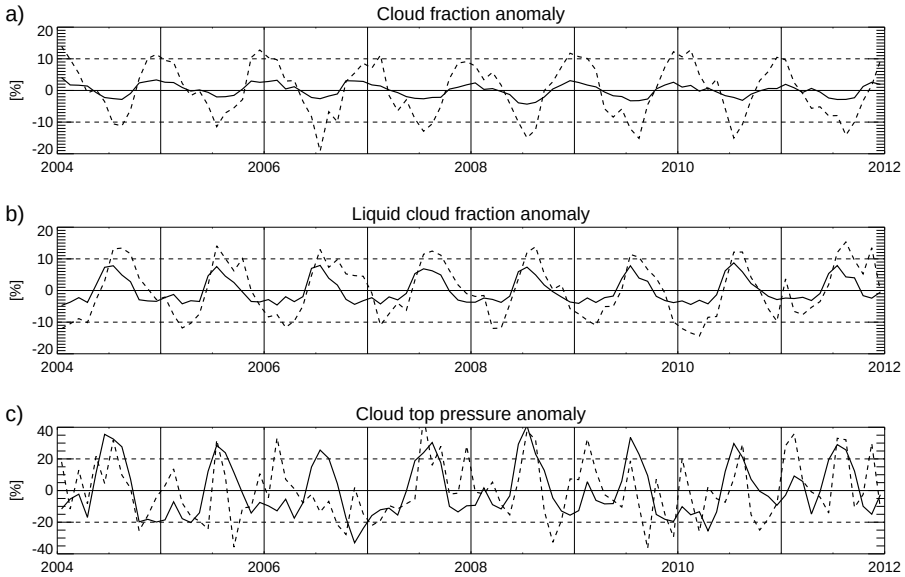

Fig. 7. Time series of CLAAS relative monthly mean anomaly of cloud fraction **(a)**, liquid cloud fraction **(b)** and cloud top pressure **(c)**, averaged over all valid retrievals within the SEVIRI disk (solid lines) and for Europe (dashed lines).

ACPD
13, 26451–26487, 2013

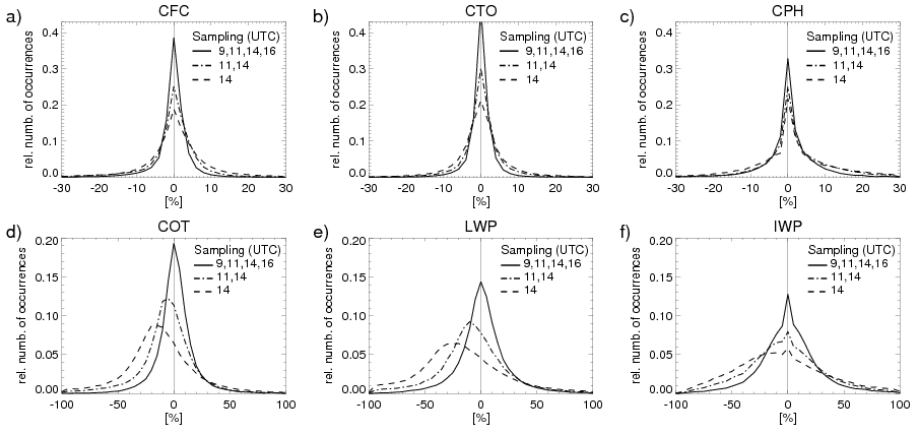

Fig. 8. Relative deviations of monthly means inferred from reduced temporal sampling with respect to the all-day average, for which all available time slots were used. Panels **(a)** through **(f)**: cloud fraction (CFC), cloud top pressure (CTO), liquid cloud fraction (CPh), cloud optical thickness (COT), liquid and ice water path (LWP and IWP). The data shown is for July 2011 and regions between −20° and 20° longitude and with satellite zenith angles lower than 72°. Note the different scaling of the axes for CFC, CTP and CPh compared to COT, LWP and IWP.

ACPD
13, 26451–26487, 2013